AJNR

Disrupted Functional and Structural Connectivity in Angelman Syndrome

H.M. Yoon, Y. Jo, W.H. Shim, J.S. Lee, T.S. Ko, J.H. Koo and M.S. Yum

AJNR Am J Neuroradiol published online 7 May 2020
http://www.ajnr.org/content/early/2020/05/07/ajnr.A6531

Published May 7, 2020 as 10.3174/ajnr.A6531

Disrupted Functional and Structural Connectivity in Angelman Syndrome

H.M. Yoon, Y. Jo, W.H. Shim, J.S. Lee, T.S. Ko, J.H. Koo, and M.S. Yum

ABSTRACT

BACKGROUND AND PURPOSE: This work investigated alterations in functional connectivity (FC) and associated structures in patients with Angelman syndrome (AS) by using integrated quantitative imaging analysis and connectivity measures.

MATERIALS AND METHODS: We obtained 3T brain MR imaging, including resting-state functional MR imaging, diffusion tensor imaging, and 3D T1-weighted imaging from children with AS ($n = 14$) and age- and sex-matched controls ($n = 28$). The brains of patients with AS were analyzed by measuring FC, white matter microstructural analysis, cortical thickness, and brain volumes; these were compared with brains of controls.

RESULTS: Interregional FC analysis revealed significantly reduced intra- and interhemispheric FC, especially in the basal ganglia and thalamus, in patients with AS. Significant reductions in fractional anisotropy were found in the corpus callosum, cingulum, posterior limb of the internal capsules, and arcuate fasciculus in patients with AS. Quantitative structural analysis also showed gray matter volume loss of the basal ganglia and diffuse WM volume reduction in AS compared with the control group.

CONCLUSIONS: This integrated quantitative MR imaging analysis demonstrated poor functional and structural connectivity, as well as brain volume reduction, in children with AS, which may explain the motor and language dysfunction observed in this well-characterized neurobehavioral phenotype.

ABBREVIATIONS: AS = Angelman syndrome; BG = basal ganglia; FA = fractional anisotropy; FC = functional connectivity; FDR = false discovery rate; M1 = primary motor area; MD = mean diffusivity; RD = radial diffusivity; rs-fMRI = resting-state functional MRI; SMA = supplementary motor area; TBSS = Tract-Based Spatial Statistics; *UBE3A* = ubiquitin protein ligase E3A; VBM = voxel-based morphometry; MNI = Montreal Neurological Institute; TCFE = threshold-free cluster enhancement

Angelman syndrome (AS) is a rare genetic disorder caused by the functional loss of ubiquitin protein ligase E3A (*UBE3A*), which arises from mutation of *UBE3A* or silencing of the maternal *UBE3A* allele. The distinctive clinical phenotypes of AS (ie, lack of expressive language development, frequent seizures, and gait abnormalities with ataxia) cause serious medical and social problems[1,2]; moreover, approximately 10% of patients with AS never achieve self-ambulation.[3] Despite their severe clinical features and well-known genetic causes, visual analysis of conventional brain MR imaging has revealed only nonspecific findings and minor abnormalities, such as mild cortical atrophy, dysmyelination, focal white matter signal abnormalities, cerebral atrophy of frontotemporal areas, and callosal thinning.[4-7]

Recently, many functional MR imaging studies have investigated the abnormal neural connectivity in patients with speech disorders or ASD[8,9] to identify the neural correlates of these functional deficits. However, there is no study to investigate an abnormal functional network in children with AS, which is a relatively homogeneous disease with a clear clinical and genetic delineation. Although WM pathway alteration and gray matter volume loss in patients with AS were previously reported by using diffusion tensor imaging and voxel-based morphometry

Received October 23, 2019; accepted after revision March 16, 2020.

From the Department of Radiology and Research Institute of Radiology (H.M.Y., W.H.S., J.S.L., J.H.K.), Asan Institute for Life Sciences (Y.J., W.H.S.), Asan Medical Center; and Department of Pediatrics (T.S.K., M.S.Y.), Asan Medical Center Children's Hospital, University of Ulsan College of Medicine, Seoul, Korea.

H.M. Yoon, Y. Jo, and W.H. Shim contributed equally to this study as the first author.

This research was supported by Basic Science Research Program through the National Research Foundation of Korea (NRF-2017R1D1A1B03030713) and Asan Institute for Life Sciences, Asan Medical Center (2018-551).

Please address correspondence to Mi-Sun Yum, Department of Pediatrics, Asan Medical Center Children's Hospital, University of Ulsan College of Medicine, 88 Olympic-ro 43-gil, Sonpa-gu, Seoul, Republic of Korea; e-mail: misun.yum@gmail.com

Indicates open access to non-subscribers at www.ajnr.org
Indicates article with supplemental on-line table.
Indicates article with supplemental on-line photos.
http://dx.doi.org/10.3174/ajnr.A6531

(VBM),[10-13] it remains unclear whether alterations in functional connectivity (FC) are related to structural deformation in AS.

Based on previous studies,[2,5] we hypothesized that the structural and FC of the fronto-striatal circuits, including language and sensorimotor domains, would be seriously compromised in patients with AS. Thus, we aimed to investigate the abnormal functional network in children with AS, which is associated with severe speech and motor deficits and to validate the key anatomic structures associated with functional loss of *UBE3A* by using multimodal quantitative MR imaging analysis.

METHODS

Participants

We enrolled patients who were clinically and genetically diagnosed with AS between July and November 2016. Eligibility criteria included (1) patients who were genetically confirmed with AS, (2) patients whose ages were less than 18 years old, and (3) patients who had no contraindications to brain MR imaging. Because most patients lack expressive language and have severe intellectual disability lower than 2 years of mental age, it was difficult to assess the patients' developmental status by using a standardized mean. The patients' motor and language functions were evaluated by an experienced pediatric neurologist (M.S.Y. with 15 years of clinical experience in pediatric neurology) at the time of their brain MR imaging. Patients were classified into 2 groups according to the severity of their verbal and motor functional status: 1) patients with no verbal output versus patients who can speak at least 1 word and 2) patients who are unable to walk unassisted versus patients who can walk unassisted.

Age- and sex-matched control subjects, with a patient to control ratio of 1:2, were retrieved from the retrospective database in our institution (Asan Medical Center) from May 2014 to July 2017. The institutional review board allowed the researchers to conduct the analysis of the MR data from this database without subject consent because the data were subject to anonymization. All patient data were anonymized when received before analysis. Children who were included in the control group were required to 1) have no alleged neurologic or psychiatric deficits, 2) be prescribed no regular medication, 3) have no abnormality on brain MR imaging, and 4) show clinically normal development. In total, 28 children (male:female = 14:14) were included, with a mean age of 7.7 ± 4.2 years (range, 1–16 years). They underwent brain MR imaging due to headache ($n = 15$), provoked seizures ($n = 7$), syncope ($n = 3$), dizziness ($n = 1$), tic disorder ($n = 1$), and minor head trauma ($n = 1$).

Written informed consent was obtained from the legal guardians of all patients. This study was performed in accordance with the ethical standards of the Declaration of Helsinki and was approved by the institutional review board of the Asan Medical Center (2016–0279, Seoul, Korea).

Imaging Protocol

All participants successfully underwent brain MR imaging by using a 3T MR imaging scanner (Achieva; Philips Healthcare, Best, The Netherlands) with an 8-channel, sensitivity-encoding head coil. 3D T1-weighted imaging sequences were acquired with the following image parameters: TR/TE, 9.9/4.6 ms; flip angle = 8°; FOV = 224 mm, matrix = 224 × 224 mm, section thickness = 1 mm with no gap; and scan time, 4 min, 41 seconds. DTI was performed by using single-shot echo-planar imaging with the following parameters: TR/TE, 5615/70 ms; section thickness, 3 mm; diffusion directions, 32; b-value, 1000 seconds/mm^2; number of excitations, 1; matrix, 112 × 112; FOV, 224 mm; acquired voxel size, 2 × 2 × 3 mm; and scan time, 3 min, 17 seconds. Blood oxygen level–dependent contrast functional images at rest (resting-state functional MR imaging [rs-fMRI]) were acquired by using single-shot gradient-echo/EPI with the following parameters: TR/TE, 3000/30 ms; flip angle, 90°; FOV, 224 mm; matrix, 112 × 112; section thickness, 6 mm with no gap; number of slices, 17; number of dynamics, 150; and acquisition time, 7 min, 42 seconds. Sedation during MR imaging examination was performed by trained anesthesiologists in accordance with our standard institutional protocol. All participants in the AS group were sedated by using intravenous administration of propofol, and children in the control group were sedated by using intravenous administration of propofol or oral chloral hydrate. Ten children in the control group did not require sedation during MR imaging examination.

Seed-Based Resting-State Functional MR Analysis

Before statistical analysis, rs-fMRI data were preprocessed by using the Analysis of Functional Neuro Images (AFNI; http://afni.nimh.nih.gov/afni) basic ANATICOR program to remove artifacts and normalize the image data.[14] In brief, we removed the first 3 EPIs to control for error, aligned the EPIs, corrected for section-time acquisition, realigned for motion correction, co-registered the EPI to anatomical T1WI, and bandpass filtered from 0.01 to 0.1 Hz.

Anatomic segmentations of 42 subjects were created by using FreeSurfer and were used to mask the following regions for FC analysis: thalami, basal ganglia (BG), primary motor area (M1), supplementary motor area (SMA), sensory area, Broca area (Brodmann area 44 and 45), and Wernicke area (superior temporal gyrus) in the left and right hemispheres. Previous studies with patients with AS[2,5,11] indicated severe speech impairment and difficulty in motor controls as well as volume reduction of the BG. The associated anatomic areas were selected as seed regions based on these clinical phenotypes of patients with AS.

Pearson correlation coefficients were calculated by using the Matlab (Matlab 8.2.0.701; MathWorks, Natick, Massachusetts) corr function between the hypothesis-derived, selectively masked regions to indicate the strength of FC between the 2 regions, producing a 14-by-14 matrix for each subject. Individual subjects' correlation matrices were then grouped into control and patient groups, and the patient group's FC was compared with that of the control group by using 2-sample t-tests after testing for equal variance (false discovery rate [FDR] corrected; $P < .05$).

Tract-Based Spatial Statistics

The DTI original time-series data were corrected for head movement and eddy current distortions by using the "eddy_correct" function within the FMRIB Diffusion Toolbox (http://fsl.fmrib.ox.ac.uk/fsl/fslwiki/FDT). The FMRIB DTIFit module (http://fsl.fmrib.ox.ac.uk/fsl/fsl-4.1.9/fdt/fdt_dtifit.html) was used to independently fit the diffusion tensors to each voxel, creating an output of voxelwise maps of fractional anisotropy (FA) for each

Table 1: Clinical characteristics of children with Angelman syndrome in this study

Characteristic	Angelman Syndrome ($n = 14$)	
Age (months)	95.9 ± 57.8 (range, 3–18 years)	
Sex (male:female)	7:7	
Genetic mutation	*UBE3A* (15q11-q13 deletions)	13
	Paternal UPD	1
Seizure	10 (71.4%)	
Use of at least 1 meaningful word	5 (35.7%)	
Walking alone	11 (78.6%)	
Ataxia or tremor	10 (71.4%)	
Strabismus	5 (35.7%)	
Ataxia and unable to walk alone	3 (21.4%)	
Ataxia but walking alone	7 (50.0%)	
No ataxia (walking alone)	4 (28.6%)	

Note: UPD indicates uniparental disomy.

subject. To limit the result to be strictly pertinent to the subject's brain, we obtained a binary brain mask from each participant's B0 image with the FSL Brain Extraction Tool's (http://fsl.fmrib.ox.ac.uk/fsl/fslwiki/BET) bet2 function and applied the brain mask to mask-out structures external to the subject's FA map.

Diffusion MR imaging data were analyzed by using FMRIB's Diffusion Toolbox Tract-Based Spatial Statistics (TBSS; v1.2; https://fsl.fmrib.ox.ac.uk/fsl/fslwiki/TBSS) module, which used the FA, mean diffusivity (MD), and radial diffusivity (RD) maps of each participant.[15] All FA images were preprocessed using TBSS's tbss_1_preproc command to further clean the FA images. Next, all FA images were registered to the MNI space by using nonlinear registration (tbss_2_reg), and the group mean FA image and WM skeleton were created by averaging all FA images (tbss_3_postreg -S), which represents the center of all WM tracts common to the group. For each individual, the local FA maxima were found along the perpendicular direction of the mean FA image and then projected onto the mean FA skeleton using a FA threshold of 0.2 (tbss_4_prestats 0.2). With the randomization function in the FMRIB Diffusion Toolbox, the skeletonized FA images were subjected to voxelwise, cross-subject statistical analysis. MD and RD maps were measured by running the FSL tool tbsds_non_FA script. Here, the mean skeletons of the control and AS groups were compared using voxelwise 2-sample unpaired t-tests with nonparametric permutation with threshold-free cluster enhancement (TFCE) corrections by using the T2 option and cluster-based thresholding at 0.95 ($P < .05$) in the randomize function (5000 permutations/design, TFCE-corrected $P < .05$ for significance).

Cortical Thickness and Volume Measurements

Entire cortex analyses were computed to explore local cortical thicknesses and cortical volumes in the AS and control groups. Statistical maps were generated with the Query, Design, Estimate, Contrast interface within FreeSurfer (version 5.3.1) used to perform group averaging and inference on cortical morphometric data. For each hemisphere, a general linear model was computed vertex by vertex for analysis of cortical thickness and cortical volume, respectively, and for regression to exclude the covariate of age. Cortical maps were smoothed with a 10-mm full width at half maximum Gaussian filter and multiple comparisons were corrected by FDR with a P value set at $<.05$. Comparisons of segmented brain volumes between subgroups in the AS group were analyzed using Mann-Whitney U tests in commercial statistical software (SPSS, version 21; SPSS; IBM, Armonk, New York). A P value less than 0.05 was considered statistically significant.

Voxel-Based Morphometry

VBM analysis in SPM8 software (http://www.fil.ion.ucl.ac.uk/spm/) was performed with the VBM technique by adhering to the standard VBM processing routine. Images of each subject were normalized and registered to MNI space; the resulting images were modulated (without the affine component) and smoothed with a full width at half maximum of 10 mm. Measurements for the transformed GM and WM images were then clustered with a threshold over 20 voxels. The final processed images were used for statistical inference; age as a covariate measure was excluded by regression with the GLM. Statistical nonparametric mapping with 5000 permutations, without variance smoothing, was used to compare voxelwise differences in GM volumes between the AS and control groups. The level of significance in SPM was considered a P value $<.001$, and multiple comparisons were corrected with family-wise error rate.

RESULTS

Patient Characteristics

A total of 14 patients (male:female =7:7) were enrolled in this study. The mean age of the patient group was 7.6 ± 4.7 years (range, 3–18 years). All patients were genetically confirmed with AS; microdeletion within chromosome 15q11-q13 in 13 patients and paternal uniparental disomy in 1 patient. Most patients initially presented with developmental delay and hypotonia. Clinical phenotypes of the enrolled patients are shown in Table 1. Among 10 patients who had seizures, 2 had histories of myoclonic status in nonprogressive encephalopathies or intractable epilepsy.

Interregional Functional Connectivity between Language, Motor, and Subcortical Areas

Fourteen seeds were placed in bilateral thalami, BG, M1, SMA, sensory, Broca, and Wernicke areas. General reduction of interregional FC was found in the AS group compared with the control group (Fig 1). In terms of interhemispheric FC, interregional FC between the left thalamus and all seeds of the right hemisphere, as well as FC between the left BG and all seeds of right hemisphere except for the right sensory area, was significantly reduced in patients with AS compared with the control group. In addition, significant reduction of interhemispheric FC between the right thalamus and left M1, sensory, and Broca areas and of FC between the right BG and left Broca area were observed in patients with AS. Regarding intrahemispheric FC of the right hemisphere, interregional FC of thalamocortical networks (thalamus and M1, Broca, Wernicke), BG and cortical networks (M1, SMA, Broca,

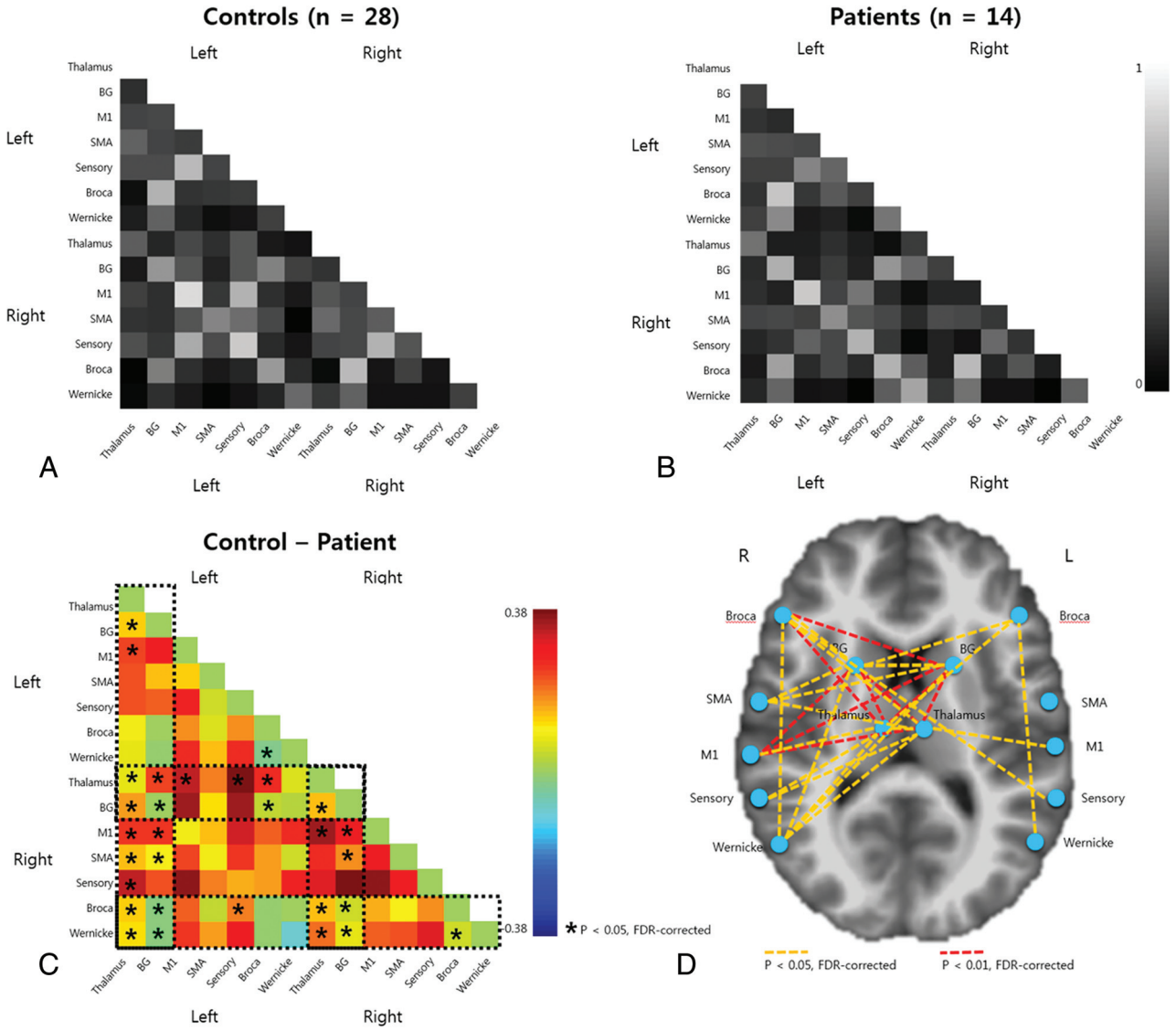

FIG 1. Correlation matrices representing functional connectivity between seed regions; (*A*) control group, (*B*) AS group, (*C*) subtraction map of A – B with *asterisks* identifying significantly different connections between A and B (FDR-corrected, $P < .05$), and (*D*) significantly reduced functional connections marked as an asterisk placed on an MNI template for visualization (*blue circle*: seed region; *yellow dotted line*: FDR-corrected, $P < .05$; *red dotted line*: FDR-corrected, $P < .01$).

Wernicke), and the language network (Broca and Wernicke areas) was significantly decreased in patients with AS. Among left intrahemispheric interregional FC, there were significant FC reductions between thalamus and BG, between thalamus and M1, and between Broca and Wernicke areas in patients with AS (all $P < .05$, FDR-corrected).

To test the effect of sedation during rs-fMRI, the Pearson correlation coefficients between patients with AS (all sedated) and sedated controls patients and the Pearson's correlation coefficients between sedated controls and nonsedated controls were compared (On-line Fig 1). Using unpaired 2-sample t-tests, we found no significant FC differences between the sedated and nonsedated controls, and the FC reduction in patients with AS showed similar results when compared with all controls (age and sex matched; $n = 28$; Fig 1; FDR-corrected, $P < .05$) or sedated controls (younger, age 3–13 years; sex matched; $n = 10$) (On-line Fig 1; FDR-corrected, $P < .05$).

Tract-Based Spatial Statistics

TBSS showed a significant FA decrease in the medial superior corpus callosum, cingulum, bilateral posterior limb of the internal capsules, corticospinal tract, cerebral peduncle, and arcuate fasciculus in the patient group compared with the control group (threshold $P < .005$ TFCE corrected, obtained using the FMRIB Software Library tool tbss_fill; Fig 2). The anatomic locales with the reduced FA were identified by using AFNI's whereami function with matching MNI coordinates, of which the MNI atlas was used for image registration. MD and RD were also analyzed in the bilateral anterior corpus callosum, posterior limb of the internal capsules, and arcuate fasciculus and posterior corpus callosum (On-line Table). All but the mean MD in bilateral posterior limb of internal capsule and posterior corpus callosum showed significant increases in the AS group.

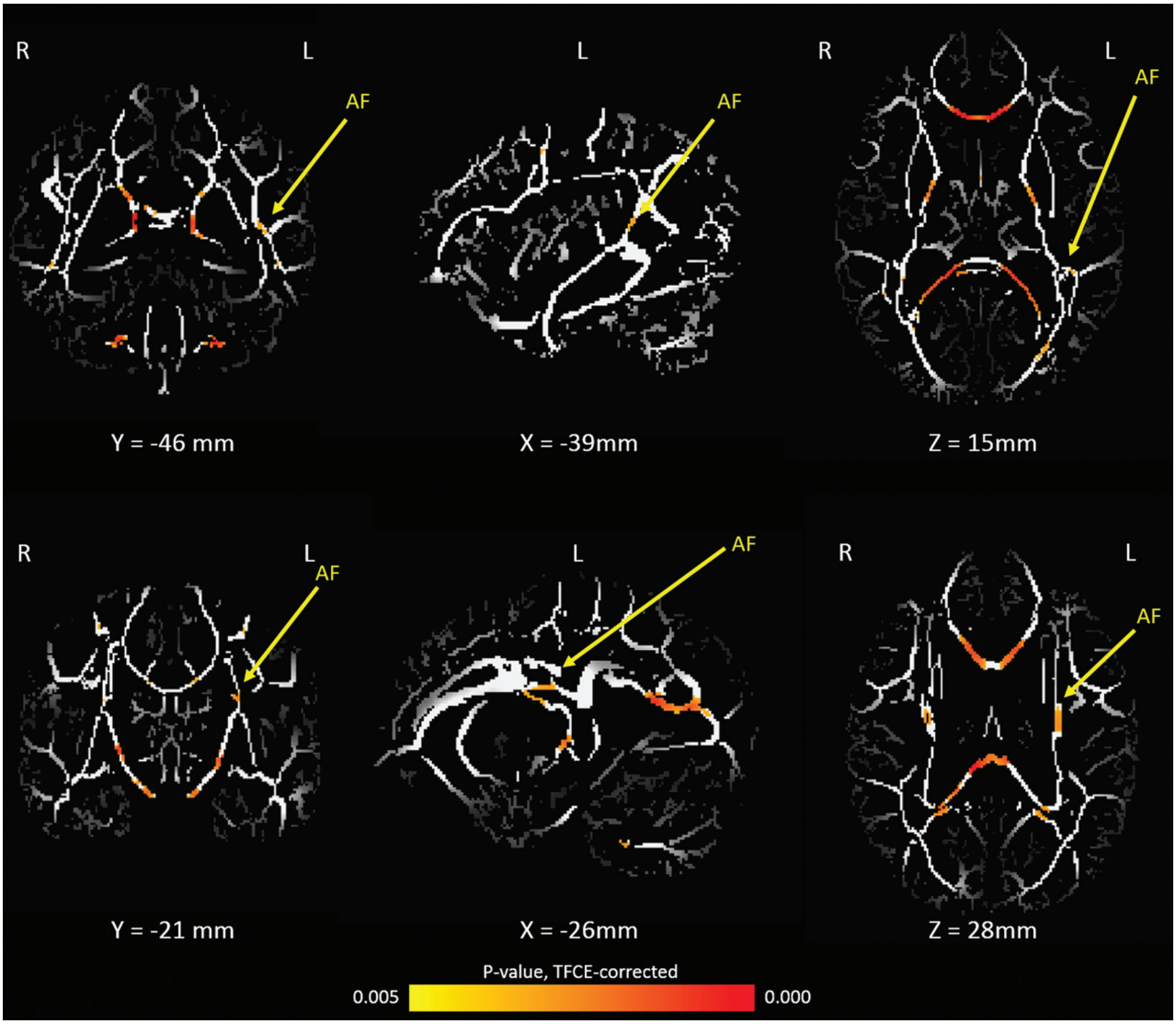

FIG 2. Regions with reduced FA in patients with AS compared with age-matched controls, determined by whole brain TBSS. The results show regions that are significantly different with the threshold of TFCE corrected, $P < .005$. The FA values of corpus callosum and arcuate fasciculus (*yellow arrows*) are significantly reduced in patients with AS.

Table 2: Cortical thicknesses of children with Angelman syndrome compared with the control group

Area Label	Brodmann Area	Size (mm^2)	Stereotactic Coordinates (Talairach Space)			T ($-Log_{(10)}P$)
			x	y	z	
Left hemisphere						
Transverse temporal	22	154.89	−51.1	−16.4	4.4	−4.9827
Postcentral	4	77.17	−60.1	−6.7	10.8	−4.7438
Superior temporal	21	86.13	−50.7	−14.6	−11.9	−4.2409
Right hemisphere						
Superior temporal	10	39.51	55.8	2.8	−12.3	−4.1946
Postcentral	1	9.20	63.6	−8.9	12.6	−3.8439
Supramarginal	40	37.79	48.0	−23.9	20.5	−3.8319
Superior frontal	8	13.04	11.3	21.6	37.7	−3.8079

Cortical Thickness and Volume Alteration

Altered Cortical Thickness in Patients with Angelman Syndrome. Compared with the control group, the AS group showed significantly smaller cortical thickness in bilateral superior temporal, bilateral postcentral, left transverse temporal, right supramarginal, and right superior frontal gyrus when using Mann-Whitney *U* tests (Table 2; FDR-corrected, $P < .05$).

Altered Brain Volume in Patients with Angelman Syndrome. In patients with AS, the global GM volume (mean ± SD of patients with AS versus control group, 600,625.8 ± 62,103.7 mm^3 versus 723,046.5 ± 53,590.5 mm^3; *t*, −4.83; *df*, 40; $P < .0001$), cerebral WM volume (306,694.5 ± 45,254.5 mm^3 versus 390,684.4 ± 60,945.5 mm^3; *t*, −4.05; *df*, 40; $P < .0001$), brain segmentation volume (941,639.3 ± 94,951.1 mm^3 versus 1,155,856.0 ± 103,920.5 mm^3; *t*, −5.08; *df*, 40; $P < .0001$), total intracranial volume (1,212,398.8 ± 132,858.0

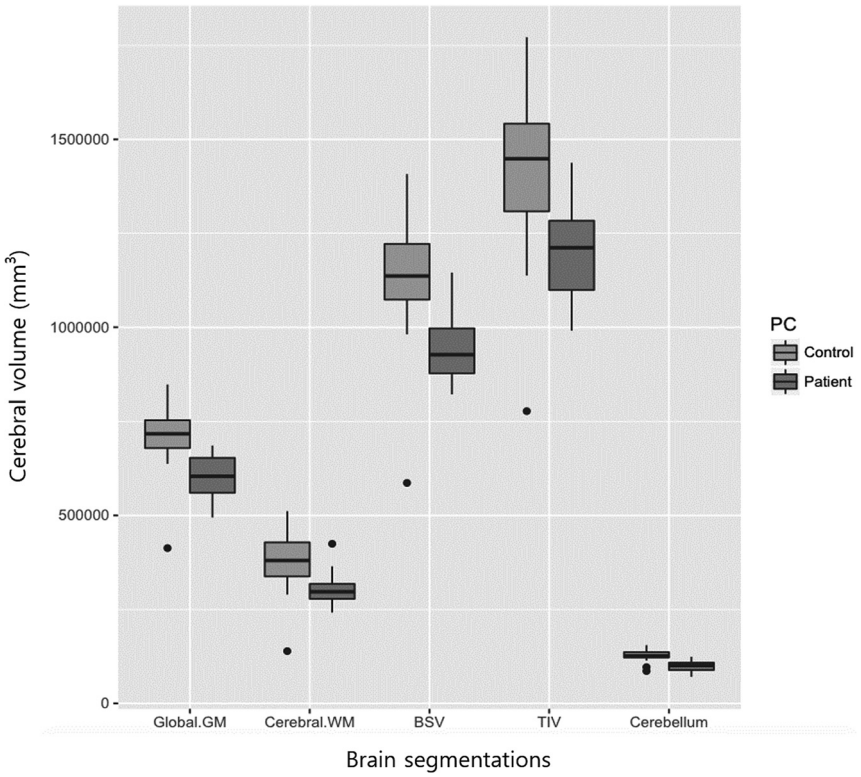

FIG 3. Boxplot for segmented volume (mm^3) of the global GM, cerebral WM, brain segmentation volume (BSV), total intracranial volume (TIV), and cerebellum. The AS group (*dark gray box*) shows significantly reduced volume of the global GM, cerebral WM, BSV, TIV, and cerebellum compared with the age-matched control group (*light gray box*). y-axis = mm^3; *black dots* = outliers.

mm^3 versus 1,442,983.0 ± 174,949.8 mm^3; *t*, −3.90; *df*, 40; $P < .0001$) and cerebellar volume (99,621.8 ± 15,085.7 mm^3 versus 127,993.0 ± 12806.0 mm^3; *t*, −5.69; *df*, 40; $P < .0001$) decreased significantly compared with those of the control group. No significant difference was found in the global CSF volume between the 2 groups (14,668.07 ± 5,554.20 mm^3 versus 15,084.69 ± 5,661.31 mm^3; *t*, −0.22; *df*, 40; $P = .821$) (Fig 3). In subgroup analysis, volumes of cerebral WM and corpus callosum were smaller in patients with no verbal output compared with patients who can speak at least 1 word (Fig 4, upper 5 boxplots). In addition, patients who are unable to walk unassisted showed smaller volumes of total GM, cortex, central portion of corpus callosum, right cerebellar cortex, and left amygdala compared with patients who can walk unassisted (Fig 4, lower five boxplots).

Voxel-Based Morphometry

Gray Matter Volume Loss in Patients with Angelman Syndrome. Regional GM volume loss was found in the AS group compared with the control group (Table 3, On-line Fig 1). Using statistical nonparametric mapping with age regressed out as a covariate measure using the general linear model (5000 permutations; $P < .001$ corrected for family-wise error rate), we found regional volumes of the bilateral putamen, globus pallidus, caudate nucleus, rectus gyrus, left hippocampus, and left cerebellar cortex were significantly reduced in the AS group compared with the control group.

White Matter Volume Loss in Patients with Angelman Syndrome. In the AS cohort, we found significant WM volume loss in the pons, anterior commissure, splenium of the corpus callosum, bilateral subinsular WM, right frontal subcortical WM, and bilateral parietal periventricular WM (On-line Fig 2) compared with the control group. These results were also found by using statistical nonparametric mapping with 5000 permutations and age excluded as a covariate measure by using the general linear model ($P < .001$, corrected for family-wise error rate).

DISCUSSION

This study used a multimodal imaging approach to study patients with AS with severe speech impairment and motor deficits. With combined use of rs-fMRI and quantitative structural imaging analysis, we attempted to define functional brain network changes in AS and compare these functional changes with the structural changes observed in these children. Children with AS exhibited significantly decreased FC in multiple intra- and interhemispheric networks; this altered FC substantially correlated with specific volume deficits in patients with AS.

In rs-fMRI analysis, children with AS showed a general decrease in interregional FC when we focused the seeds in areas associated with primary motor and language systems. Especially, intra- and interhemispheric FC associated with the thalamus and BG of patient with AS were significantly decreased compared with controls. Considering the role of the BG and the thalamus network in motor control and balance,[16,17] altered FC mainly involving thalamus and BG might be related to the impaired motor function in patients with AS. Furthermore, BG volume was smaller in the AS group than the control group in VBM analysis. In a murine AS model, *ube3a* reinstatement could alleviate the AS-relevant phenotypes.[18] However, cerebellum-specific reinstatement of *ube3a* in AS mice alone could not rescue the locomotor deficits, which suggests the role of other structures, such as the BG, in locomotor dysfunctions of AS.[19]

Regarding the language network, interregional FC between the Broca and Wernicke areas in each hemisphere was significantly reduced in the AS group. In TBSS analysis, the AS group also showed significant reductions in FA in the arcuate fasciculus, which connects the Broca and Wernicke areas; this was consistent with previous reports.[12] This association between functional and structural alteration in the language network may be associated with impairment of language function in patients with AS. In addition, the language network demonstrated decreased interregional FC with the thalamus and BG, intra- and

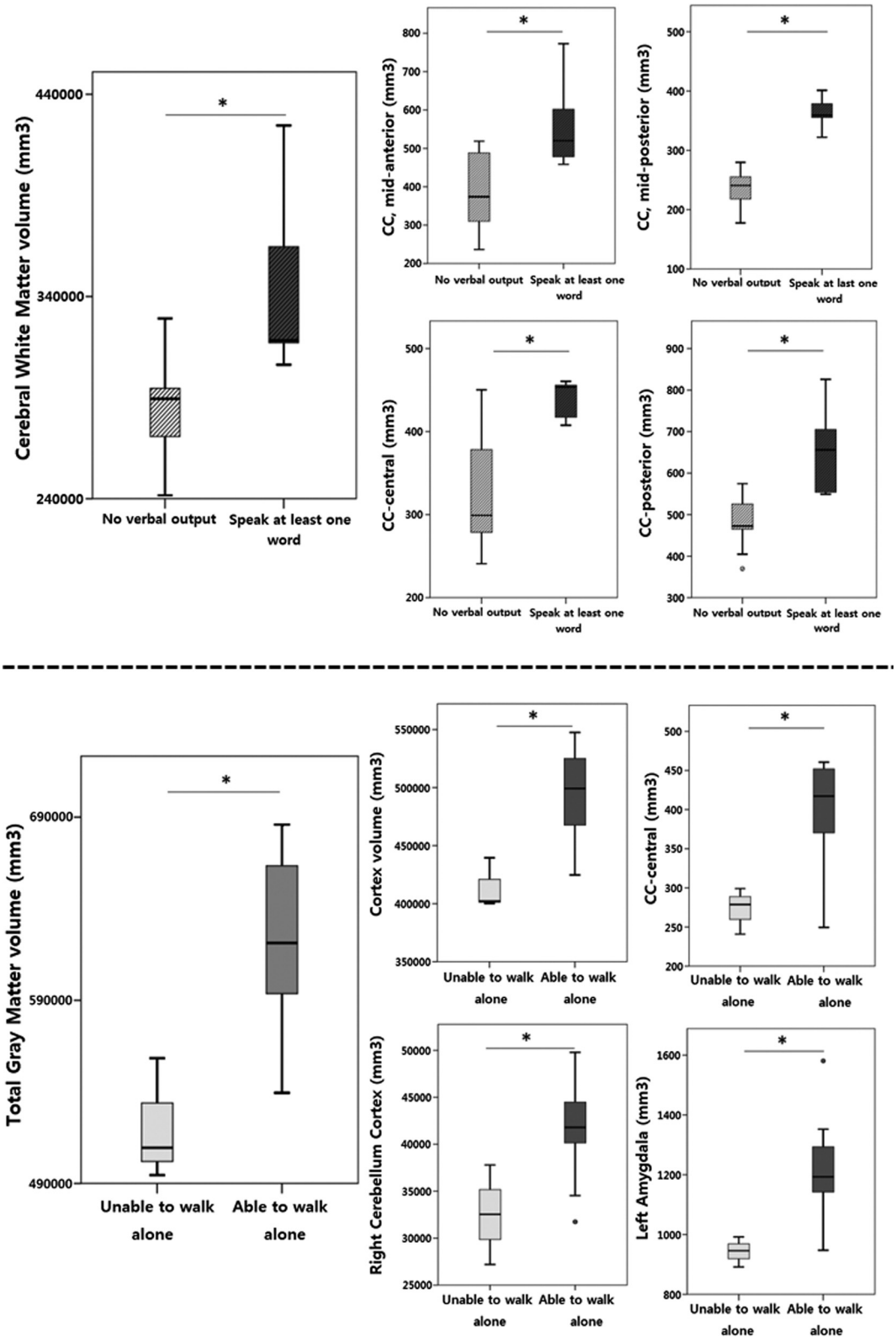

FIG 4. Upper 5 plots: boxplots for segmented volume (mm^3) of the cerebral white matter and segments of the corpus callosum. Patients with no verbal output (*gray box*) show significantly reduced volume of aforementioned areas compared with patients who can speak at least a word (*black box*). Lower 5 plots: boxplots for segmented volume (mm^3) of the total gray matter, cortex, corpus callosum (central), right cerebellum cortex, and left amygdala. Patients who were unable to walk alone (*light gray box*) have significantly reduced volume of aforementioned areas compared with patients who can walk alone (*gray box*). *Asterisks* indicate significant difference ($P < .05$). y-axis = mm^3.

Table 3: Regional gray matter volume reductions in patients with Angelman syndrome compared with controls based on voxel-based morphometry analysis[a]

Anatomic Region	Number of Voxels in Each Cluster	Peak *Z* Score	Coordinates of Voxel of Maximal Statistical Significance (MNI Space)
Left putamen, pallidum, caudate nucleus	18,317	7.73	−21, 2, 12
Right caudate nucleus		7.68	9, 11, 15
Right putamen, pallidum		7.66	21, 5, 12
Right rectal gyrus	469	6.16	9, 34,−26
Right superior orbital gyrus			
Left rectal gyrus			
Left hippocampus	159	5.96	−20, −34, −0
Left thalamus			
Left parahippocampal gyrus			
Left lingual gyrus			
Left cerebellum (Crus 1, 2)	156	5.95	−51, −48, −36
Left cerebellum (VII, VIII, crus 2)	47	5.67	−46, −43, −50
Left rectal gyrus	28	5.58	−6, 36, −30
Right rectal gyrus			
Left superior orbital gyrus			

[a]Whole-brain analysis (FWE-corrected at $P < .001$; cluster threshold >20 voxels).

interhemispherically; these changes were more prominent in the right hemisphere. The BG, including dorsal striatum, is involved in language processing[20]; however, the role of the thalamus in language function remains controversial.[21] Altered FC in the language network and BG or thalamus may be associated with impairment of language function in patients with AS.

TBSS analysis also showed significant overall reductions in FA in the corpus callosum, arcuate fasciculus, and corticospinal tracts, as in a previous report.[12] Additional analysis of other metrics of DTI showed significant increased MD and RD in these areas (On-line Table). Furthermore, consistent with broad structural connectivity abnormalities of patients with AS, VBM analysis in this study showed diffuse WM volume reduction in patients with AS, including the pons, anterior commissure, splenium of the corpus callosum, bilateral subinsular, and parietal periventricular areas. These WM volume reductions, as well as the reduced WM microstructural connectivity, can mirror behavioral phenotypes in AS. Similarly, research involving the murine model of AS showed that dysfunctional *ube3a* causes alteration in the intrinsic properties of membranes and axons[22] and the disproportional loss of WM volumes and lowered integrity, as well as smaller axon caliber.[23]

Together with this global reduction of functional and structural connectivity, as well as WM volume reduction in AS, VBM analysis also showed consistent cerebral and cerebellar volume reductions in patients with AS. In the human cortex, *UBE3A* is expressed in both glutamatergic, GABAergic neurons and glial cells,[24] which suggests that *UBE3A* dysregulation might affect the whole neuronal circuit. Considering the symptoms of AS (ie, severe speech impairment, unique puppet-like movement, autistic features), the global reduction of brain volume as well as the abnormal FC is deemed reasonable. When we divided the patients into subgroups according to motor and language function to test whether anatomic change can be used as an imaging biomarker for these neurobehaviors, patients with poor language or motor function showed smaller cortical WM or GM volumes. These subgroups consisted of a smaller number of subjects, and further investigation is required. However, these findings provide further evidence that quantitative brain MR imaging may demonstrate functional deficits in AS.

When compared with the age- and sex-matched children with normal development, patients with AS exhibited cortical thinning of the superior temporal and transverse temporal gyri, the area of primary auditory cortex involved in auditory processing, including language sense and social cognition.[25] The thinning of the right superior frontal gyrus, which mediates the inhibitory control of impulsive behavior,[26] and the supramarginal gyrus, a part of the somatosensory association cortex with a mirror neuron system,[27,28] were also observed by cortical thickness analysis.

Nonetheless, this study has several limitations. First, the number of patients was small. This syndrome is quite rare; furthermore, recruitment of patients for MR imaging examination is difficult because many parents or guardians of the patients tend to be reluctant to make their children undergo MR imaging because of sleep and behavioral problems, which are closely associated with each other. After sedation, sleep disturbances in patients with AS can be exacerbated by sleep cycle changes, which can lead to behavioral deterioration. Second, different sedation protocols were applied in the control and AS groups. It has been shown that the FC of several brain networks can be influenced by sedative drugs used for MR imaging.[29,30] Sedation was inevitable for all patients with AS because of severe communication difficulties; older children in the control group did not need sedation during MR imaging. However, it is unethical to make normal children undergo brain MR imaging under sedation. These heterogeneities in sedation protocol may affect our results, especially rs-fMRI data. Although the pattern of FC difference was similar when we excluded the nonsedated patients, the effect of age, sex, and sedation should be carefully considered. Last, the control group in this study had minor neurologic symptoms, such as headache or febrile seizures, which might also affect our results. Further studies with a homogeneous sedation protocol and control group without any neurologic symptoms are required to confirm our preliminary results.

CONCLUSIONS

We found reduced brain connectivity with associated anatomic structural changes in children with AS. Functional and structural underconnectivity, as well as diffuse brain volume reduction, shown by MR imaging may provide striking imaging evidence for the impairment of motor and speech ability seen in individuals with AS.

ACKNOWLEDGMENTS

We thank all of the patients and families involved in this study and the biomedical computing core facility at the ConveRgence

mEDIcine research cenTer (CREDIT), Asan Medical Center for support and instrumentation.

Disclosures: Woo-Hyun Shim—*RELATED: Grant*: This research was supported by Basic Science Research Foundation of Korea (NRF) funded by the Ministry of Education (2017R1D1A1B0303713). Mi-Sun Yum—*RELATED: Grant:* This research was supported by Asan Institute for Life Sciences, Asan Medical Center (2018-551).* *Money paid to institution.

REFERENCES

1. Lalande M, Calciano MA. **Molecular epigenetics of Angelman syndrome.** *Cell Mol Life Sci* 2007;64:947–60 CrossRef
2. Williams CA. **The behavioral phenotype of the Angelman syndrome.** *Am J Med Genet C Genet* 2010;154C:432–37 CrossRef
3. Buiting K, Williams C, Horsthemke B. **Angelman syndrome—insights into a rare neurogenetic disorder.** *Nat Rev Neurol* 2016; 12:584–93 CrossRef
4. Clayton-Smith J. **Clinical research on Angelman syndrome in the United Kingdom: observations on 82 affected individuals.** *Am J Med Genet* 1993;46:12–15 CrossRef
5. Leyser M, Gonsalvez MCD, Vianna PES, et al. **Scrutinizing brain magnetic resonance imaging patterns in Angelman syndrome.** *Neurol India* 2016;64:228–32 CrossRef
6. Castro-Gago M, Gomez-Lado C, Eiris-Punal J, et al. **Abnormal myelination in Angelman syndrome.** *Eur J Paediatr Neurol* 2010;14:292 CrossRef
7. Harting I, Seitz A, Rating D, et al. **Abnormal myelination in Angelman syndrome.** *Eur J Paediatr Neurol* 2009;13:271–76 CrossRef
8. Rashid B, Blanken LME, Muetzel RL, et al. **Connectivity dynamics in typical development and its relationship to autistic traits and autism spectrum disorder.** *Hum Brain Mapp* 2018;39:3127–42 CrossRef
9. Morgan A, Bonthrone A, Liegeois FJ. **Brain basis of childhood speech and language disorders: are we closer to clinically meaningful MRI markers?** *Curr Opin Pediatr* 2016;28:725–30 CrossRef
10. Peters SU, Kaufmann WE, Bacino CA, et al. **Alterations in white matter pathways in Angelman syndrome.** *Dev Med Child Neurol* 2011;53:361–67 CrossRef
11. Aghakhanyan G, Bonanni P, Randazzo G, et al. **From cortical and subcortical grey matter abnormalities to neurobehavioral phenotype of Angelman syndrome: a voxel-based morphometry study.** *PLoS One* 2016;11:e0162817 CrossRef
12. Tiwari VN, Jeong JW, Wilson BJ, et al. **Relationship between aberrant brain connectivity and clinical features in Angelman syndrome: a new method using tract based spatial statistics of DTI color-coded orientation maps.** *Neuroimage* 2012;59:349–55 CrossRef
13. Wilson BJ, Sundaram SK, Huq AH, et al. **Abnormal language pathway in children with Angelman syndrome.** *Pediatr Neurol* 2011;44: 350–56 CrossRef
14. Jo HJ, Saad ZS, Simmons WK, et al. **Mapping sources of correlation in resting state FMRI, with artifact detection and removal.** *Neuroimage* 2010;52:571–82 CrossRef
15. Smith SM, Jenkinson M, Johansen-Berg H, et al. **Tract-based spatial statistics: voxelwise analysis of multi-subject diffusion data.** *Neuroimage* 2006;31:1487–505 CrossRef
16. Mestres-Misse A, Turner R, Friederici AD. **An anterior-posterior gradient of cognitive control within the dorsomedial striatum.** *Neuroimage* 2012;62:41–47 CrossRef
17. Patel N, Jankovic J, Hallett M. **Sensory aspects of movement disorders.** *Lancet Neurol* 2014;13:100–12 CrossRef
18. Silva-Santos S, van Woerden GM, Bruinsma CF, et al. **Ube3a reinstatement identifies distinct developmental windows in a murine Angelman syndrome model.** *J Clin Invest* 2015;125:2069–76 CrossRef
19. Bruinsma CF, Schonewille M, Gao Z, et al. **Dissociation of locomotor and cerebellar deficits in a murine Angelman syndrome model.** *J Clin Invest* 2015;125:4305–15 CrossRef
20. Klostermann F, Krugel LK, Ehlen F. **Functional roles of the thalamus for language capacities.** *Front Syst Neurosci* 2013;7:32 CrossRef
21. Llano DA. **Functional imaging of the thalamus in language.** *Brain Lang* 2013;126:62–72 CrossRef
22. Kaphzan H, Buffington SA, Jung JI, et al. **Alterations in intrinsic membrane properties and the axon initial segment in a mouse model of Angelman syndrome.** *J Neurosci* 2011;31:17637–48 CrossRef
23. Judson MC, Burette AC, Thaxton CL, et al. **Decreased axon caliber underlies loss of fiber tract integrity, disproportional reductions in white matter volume, and microcephaly in Angelman syndrome model mice.** *J Neurosci* 2017;37:7347–61 CrossRef
24. Burette AC, Judson MC, Li AN, et al. **Subcellular organization of UBE3A in human cerebral cortex.** *Mol Autism* 2018;9:54 CrossRef
25. Bigler ED, Mortensen S, Neeley ES, et al. **Superior temporal gyrus, language function, and autism.** *Dev Neuropsychol* 2007;31:217–38 CrossRef
26. Hu S, Ide JS, Zhang S, et al. **The right superior frontal gyrus and individual variation in proactive control of impulsive response.** *J Neurosci* 2016;36:12688–96 CrossRef
27. Woo YJ, Wang T, Guadalupe T, et al. **A common cyfip1 variant at the 15q11.2 disease locus is associated with structural variation at the language-related left supramarginal gyrus.** *PLoS One* 2016;11: e0158036 CrossRef
28. Hoffmann F, Koehne S, Steinbeis N, et al. **Preserved self-other distinction during empathy in autism is linked to network integrity of right supramarginal gyrus.** *J Autism Dev Disord* 2016;46:637–48 CrossRef
29. Liu X, Lauer KK, Ward BD, et al. **Differential effects of deep sedation with propofol on the specific and nonspecific thalamocortical systems.** *Anesthesiology* 2013;118:59–69 CrossRef
30. Hashmi JA, Loggia ML, Khan S, et al. **Dexmedetomidine disrupts the local and global efficiencies of large-scale brain networks.** *Anesthesiology* 2017;126:419–30